arXiv:1609.07131v1 [cond-mat.stat-mech] 22 Sep 2016

Inferring microscopic dissipation rates from coarse-grained current fluctuations

Todd R. Gingrich,[1] Grant M. Rotskoff,[2] and Jordan M. Horowitz[1]

[1] *Physics of Living Systems Group, Department of Physics, Massachusetts Institute of Technology, 400 Technology Square, Cambridge, MA 02139*[*]

[2] *Biophysics Graduate Group, University of California, Berkeley, CA 94720*

Complex physical dynamics can often be modeled as a Markov jump process between mesoscopic configurations. When jumps between mesoscopic states are mediated by thermodynamic reservoirs, the time-irreversibility of the jump process is a measure of the physical dissipation. We review recent results to derive an inequality relating the dissipation rate to current fluctuations. We describe how the jump process results carry over to diffusion processes via a limiting procedure and reaffirm that diffusions saturate the inequality. Finally, we demonstrate the practical implications for experimental measurements. By observing fluctuations in coarse-grained currents, we show that it is possible to infer a lower bound on the total dissipation rate, including the dissipation associated with hidden dynamics.

I. INTRODUCTION

Experiments capable of probing molecular-scale dynamics have lead to a wealth of data about the operation of nanoscale machines [1–3]. Like their macroscopic counterparts, nanomachines convert free energy from the environment into useful work. However, due to molecular fluctuations they behave stochastically. These fluctuations make the machine less predictable, but they also offer a unique tool to deduce its physical properties. Indeed, classical applications of the Fluctuation Dissipation Theorem (FDT) demonstrated that the nonequilibrium response to small perturbations could be inferred from near-equilibrium fluctuations, an idea that has become a central theme of statistical mechanics [4–9]. Analogous exploitation of far-from-equilibrium fluctuations is highly desirable [10–14], particularly for studying living systems [15–17].

The dynamics of a system far from equilibrium can be analyzed by fitting observed fluctuations to an explicit model of the microscopic dynamics. For example, fluorescence correlation spectroscopy assumes free diffusion as the microscopic dynamics to determine protein diffusion constants by observing fluctuations in the number of fluorescent proteins occupying a small volume [18]. In general, however, it is difficult to find simple models that accurately describe nonequilibrium systems in terms of a small number of experimentally measurable parameters. More agnostic, high-dimensional models, on the other hand, require a prohibitive quantity and quality of experimental data. In this work, we address the challenge of extracting information from nonequilibrium fluctuations in a general setting, making minimal assumptions about the microscopic model.

Our central assumption is that mesoscopic dynamics, in a quantum or a classical system, can be described by a Markovian stochastic process. Given this mesoscale description, we use recent developments in the theory of Markov processes [19–22] to relate the physical dissipation rate to nonequilibrium dynamical fluctuations [23–25]. While the FDT offers an equality—by measuring fluctuations we may determine the dissipation exactly [26]—the far-from-equilibrium analog guarantees only an inequality: the extent of fluctuations sets a lower bound on the dissipation rate. What is more, inferring dissipation rates with this generalization of the FDT does not necessitate a parametrization of the mesoscopic dynamics. Rather, direct experimental observations of macroscopic, coarse-grained fluctuations provide enough information to estimate the dissipation rate associated with a far-from-equilibrium process.

In this paper, we develop this generalization of the FDT bound from the perspective of coarse-graining, a viewpoint which will complement experimental applications. We first review the formalism of Markov jump processes in Section II. In Section III we present a new heuristic derivation to quantify dynamical fluctuations in the jump process. Unlike prior derivations of this result [19–22], our presentation does not assume familiarity with the mathematical techniques of large deviation theory [27]. Mirroring previous work [24], Section IV develops our central relationship between nonequilibrium dynamical fluctuations and dissipation. In its most general form, the relationship pertains to fluctuating vector quantities; the implication for scalar quantities is detailed in Section V. By considering infinitely fine-grained mesostates in Section VI, we demonstrate how current fluctuations of diffusive processes become strictly Gaussian and are determined exactly by the local dissipation rates. Finally, in Section VII, we address the opposite limit by clustering mesostates into macrostates, which mimics the limited resolution of experimental data. A consequence of the coarse-graining is that the macrostate dynamics is not generally Markovian. Remarkably, even without the Markov property, coarse-grained fluctuations can bound the dissipation rate so long as the macroscopic dynamics emerges from an underlying Markovian description.

[*] toddging@mit.edu

II. MARKOV JUMPS ON GRAPHS

A. Dissipation

Before studying the consequences of coarse-graining, we first build a detailed dynamical model. At the smallest scales, the microscopic laws of physics are Markovian and, in the case of classical dynamics, deterministic. By clustering microscopic configurations into sufficiently many mesostates, mesocopic dynamics may often be described by a continuous-time Markov jump process on the set of coarse-grained states [28–30]. Such a model can be constructed, for example, from atomistic simulations, as in the case of protein conformational dynamics [31, 32]. The jump process is a random walk on a graph, with each of the N vertices corresponding to one of the possible mesostates. Fig. 1 depicts an example with twelve states. Any two vertices, y and z, are connected by an edge when the system can jump between mesostate y and mesostate z. We denote the rate for transitioning from y to z by $r(y,z)$ and require a non-vanishing rate $r(z,y)$ for the reverse transition.

The probability of occupying state y at time t, $p(y)$, evolves according to the master equation

$$\frac{\partial p(y)}{\partial t} = \sum_{y \neq z} j^p(y,z), \tag{1}$$

where $j^p(y,z) = r(y,z)p(y) - r(z,y)p(z)$ is the current passing from y to z. Following Bertini et al. [21, 22], the superscript p highlights the dependence on the density. At long times, the probability of occupying mesostate y approaches the steady state value,

$$\pi(y) \equiv \lim_{t\to\infty} p(y). \tag{2}$$

Similarly, the current passing from state y to z approaches $j^\pi(y,z) = \pi(y)r(y,z) - \pi(z)r(z,y)$ in the steady state. We will use bold symbols to represent vectors and let context distinguish whether the vector is indexed over vertices (as in $\boldsymbol{\pi}$) or edges (as in $\boldsymbol{j}^\pi$ and $\boldsymbol{r}$).

An equilibrium system obeys detailed balance, meaning that all steady state currents vanish, $\boldsymbol{j}^\pi = \mathbf{0}$. Non-vanishing currents may be generated if the system couples to multiple external reservoirs with differing intensive parameters, e.g., temperatures, pressures, or chemical potentials. The environment, which we model as a set of infinitely-large reservoirs, can therefore lead to broken detailed balance, i.e., it need not be the case that mesostates y and z satisfy $\pi(y)r(y,z) = \pi(z)r(z,y)$.

Because the mesoscopic Markov dynamics does not explicitly model the state of the thermodynamic reservoirs, e.g., how much energy and how many particles are in the baths, the impact of the reservoirs appears implicitly in the rates $\boldsymbol{r}$. As an example, suppose mesostate y has a (free) energy lower than that of mesostate z by an amount ΔE. The transfer of energy from a thermal reservoir at inverse temperature β can induce an uphill transition from y to z. If we assume the mesoscopic configurations are locally equilibrated with the thermal reservoir, then the transitions must obey detailed balance with respect to the reservoir's equilibrium distribution p_{eq} [33]. This local detailed balance condition, $p_{\text{eq}}(y)r(y,z) = p_{\text{eq}}(z)r(z,y)$, yields

$$\frac{r(y,z)}{r(z,y)} = \frac{p_{\text{eq}}(z)}{p_{\text{eq}}(y)} = \exp(-\beta\Delta E), \tag{3}$$

which relates the ratio of transition rates to the energy flux from the reservoir. These same arguments apply to other types of reservoirs, e.g., a particle reservoir at constant chemical potential. In general, we write the ratio of transition rates in terms of ΔS, the amount by which the reservoir entropy increases when the system jumps from y to z:

$$\frac{r(y,z)}{r(z,y)} = \exp(-\Delta S). \tag{4}$$

Satisfying local detailed balance with the various reservoirs does not imply that the Markov dynamics obeys detailed balance. When coupled to multiple reservoirs with incompatible equilibrium states, the Markov dynamics breaks detailed balance, but Eq. (4) still relates the mesoscopic rates to the flow of entropy from the reservoirs. We quantify the broken detailed balance by

$$F^p(y,z) = \ln \frac{p(y)r(y,z)}{p(z)r(z,y)}, \tag{5}$$

which we call the thermodynamic force because it measures how much free energy the baths must provide in order for the system to transition from y to z [34]. In the steady state the rate of that free energy transfer is given by

$$\sigma^\pi(y,z) = j^\pi(y,z)F^\pi(y,z). \tag{6}$$

We call this quantity the dissipation rate for the edge connecting y and z. The total dissipation rate for the system is computed by summing the dissipation rates for all edges:

$$\Sigma^\pi = \boldsymbol{j}^\pi \cdot \boldsymbol{F}^\pi \equiv \sum_{y<z} j^\pi(y,z)F^\pi(y,z). \tag{7}$$

We select an arbitrary ordering of mesostates and sum only over pairs of states with $y < z$ to avoid double counting.

Though straightforward, computing the dissipation rate via Eq. (7) is all-but-impossible for complicated problems. The computation requires that all possible mesostates be identified, that the rates for transitions between these mesostates be measured, and that the steady-state density be computed. Even the simplest of these tasks, identifying the sets of mesostates, is frequently impractical. More commonly, it is only possible to monitor transitions between some coarse-grained macrostates. With this limitation in mind, we set out

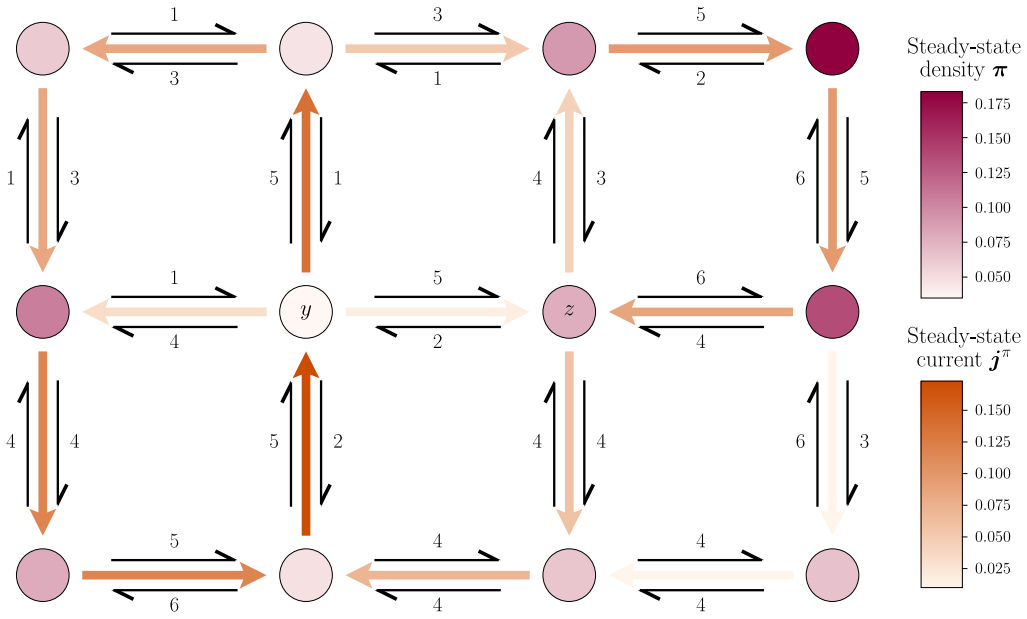

FIG. 1. Example of a Markov jump process: Mesostates are shaded according to the steady-state density $\boldsymbol{\pi}$. Black arrows on the edges label the transition rates, and the colored edges indicate the steady-state current across each edge, $\boldsymbol{j}^{\pi}$.

to infer the dissipation rate on the basis of fluctuations in finite-time stochastic trajectories. Our strategy only provides a lower bound on the dissipation rate, but may be applied even when we only observe macrostate transitions, a point we return to in Section VII.

B. Fluctuations

An infinitely long trajectory samples all configurations in proportion to the steady-state distribution, but a single finite-time trajectory has fluctuations. Consider one realization of the jump process, initialized in the steady state and observed for a long but finite time T. We let $x(t)$ denote the identity of the occupied mesostate at time t. Given this trajectory, an unbiased estimate of the steady state density at mesostate y is found by measuring the fraction of time spent in y:

$$p(y) = \frac{1}{T}\int_0^T dt\ \delta_{x(t),y}, \tag{8}$$

with Kronecker delta $\delta_{\alpha,\beta}$. This $\boldsymbol{p}$ is our empirical density. Similarly, the empirical current from y to z counts the rate of transitions from y to z, less those from z to y:

$$j(y,z) \equiv \frac{1}{T}\int_0^T dt\ \delta_{x(t^-),y}\delta_{x(t^+),z} - \delta_{x(t^-),z}\delta_{x(t^+),y}. \tag{9}$$

The notation $x(t^{\pm})$ is shorthand for the configuration immediately before or immediately after time t. Note that $j(y,z)$ differs from $j^p(y,z)$. The former reflects the number of transitions observed in a stochastic trajectory while the latter is the current that one would expect given the empirical density $\boldsymbol{p}$ and the transition rates $\boldsymbol{r}$.

Our goal is to characterize the probability of the empirical measurements of density and current, which reflect the fluctuations anticipated in finite-time experiments or simulations. For large T, the density and current adopt the large deviation form

$$P(\boldsymbol{p},\boldsymbol{j}) \asymp e^{-TI(\boldsymbol{p},\boldsymbol{j})} \tag{10}$$

with the joint rate function $I(\boldsymbol{p},\boldsymbol{j})$ measuring, on an exponential scale, the chance of observing fluctuations away from steady state density $\boldsymbol{\pi}$ and steady state current $\boldsymbol{j}^{\boldsymbol{\pi}}$ [27]. We use $\asymp$ to indicate asymptotic equivalence, meaning

$$-\frac{1}{T}\ln P(\boldsymbol{p},\boldsymbol{j}) = I(\boldsymbol{p},\boldsymbol{j}) + \mathcal{O}\left(\frac{1}{T}\right). \tag{11}$$

The rate function attains a minimum at the steady-state values ($I(\boldsymbol{\pi},\boldsymbol{j}^{\pi}) \equiv 0$) since the steady-state behavior dominates in the long-time limit. The local curvature of I around its minimum, also known as the Hessian, reveals the variance of the empirical fluctuations away from the steady-state values. Remarkably, the local curvature can be computed analytically because an explicit expression for $I(\boldsymbol{p},\boldsymbol{j})$ is known [19–22].

III. COARSE-GRAINING IN TIME —A HEURISTIC DERIVATION LONG-TIME FLUCTUATIONS

The rate function describes the distribution of empirical density and current one would measure from a collection of long trajectories. Each trajectory contains complete information about the sequence of visited mesostates, but Eqs. (8) and (9) are time-averaged quantities that have integrated out most of the temporal details. Thus by recording only the empirical density and empirical current, we have temporally coarse-grained the trajectories, and $I(\boldsymbol{p}, \boldsymbol{j})$ describes the fluctuations in the limit of an infinitely-long coarse-graining timescale. In that long-time limit, the coarse-grained Markov jump process resembles the behavior of a collection of independent Poisson point processes, one per edge of the graph. We use the asymptotic equivalence of these two processes to derive $I(\boldsymbol{p}, \boldsymbol{j})$. While this result has been rigorously derived using a technique called Cramér tilting [20], our simple approach clarifies how the form of the jump process rate function originates from a Poisson point process.

The Markov jump process has rich temporal correlations—after a short time, a system initialized in mesostate y is more likely to be in a neighboring state z than $\pi(z)$ would predict. Though these correlations add complexity to transient dynamics, they die out in some finite correlation time. Hence empirical fluctuations, averaged over long timescales, are mimicked by the Poisson point processes, which lack all temporal correlations. The large deviation structure of Poisson processes is particularly simple, providing a route to compute $I(\boldsymbol{p}, \boldsymbol{j})$ for a general nonequilibrium jump process.

To explicitly demonstrate that the Markov jump process' long-time behavior resembles that of a collection of Poisson point processes, we first focus on a single type of dynamical event—hops from mesostate y to z in Fig. 1. We record the time of each such hop by a blue tick on a timeline in Fig. 2. The average density of ticks is

$$q(y,z) = \frac{1}{T}\int_0^T dt\ \delta_{x(t^-),y}\delta_{x(t^+),z}, \tag{12}$$

the empirical flow rate from y to z [21, 22]. Due to the stochastic nature of the trajectories, the spacing between tick marks is highly variable. Immediately following each $y \to z$ event, the system is localized in mesostate z, and the next $y \to z$ event cannot occur until the system finds its way back to mesostate y. This need to reset introduces temporal correlations, quantified by the pair-correlation function

$$g(t) = \left\langle \frac{\sum_{i<j} \delta\left(t - (t_j - t_i)\right)}{q(y,z)} \right\rangle, \tag{13}$$

with t_i denoting the time of the i^{th} $y \to z$ hop. The average in the definition of $g(t)$ is taken over long trajectories of length T.

Akin to the pair correlation function of liquid state theory [35], $g(t)$ captures the probability that, given an event at time 0, another event occurs after a delay time t. The blue curve in Fig. 2 shows $g(t)$ for the flows from state y to z in Fig. 1. At short times, $g(t)$ exceeds one, indicating a propensity for bursty repeated events since the return rate $r(z,y)$ enables multiple $y \to z$ events in rapid succession. After slightly longer times, $g(t)$ is less than one; trajectories which do not backtrack from z to y only enable the next event upon returning to y via a slower, circuitous route. Finally, $g(t)$ approaches 1 for $t > \tau_{\text{corr}}$, the timescale on which correlations are lost.

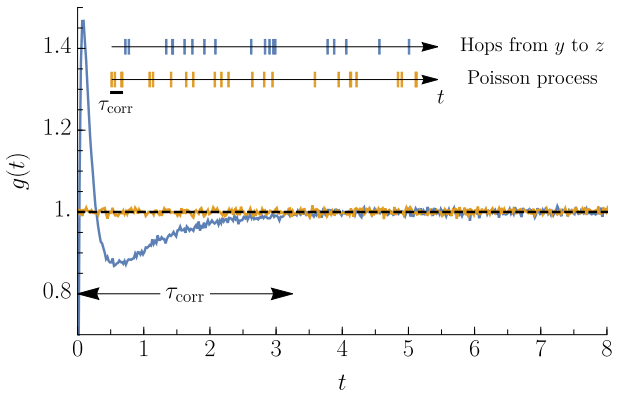

FIG. 2. Pair correlation functions $g(t)$ for Markov dynamics on the graph in Fig. 1 (blue) and for an Poisson point process (orange). Time is reported in the same units as the inverse of the rate constants in Fig. 1. The colored lines are collected by sampling from 5000 trajectories, each of length 10000; the dashed black line shows the exact result for a Poisson point process. The inset shows a timeline for the events observed in a representative trajectory, with each tick corresponding to the time of a hopping event. The Poisson point process is constructed such that it has the same average density of tick marks as the Markov dynamics on the graph. For times much larger than a correlation time τ_{corr}, the Markov dynamics hops become uncorrelated, so the fluctuations in the number of events asymptotically approaches that of the Poisson point process, Eq. (15).

These temporal correlations are an important feature of a Markov jump process at short times. However, the two-time correlations encoded in $g(t)$ become insignificant at long times, for which $g(t) \to 1$. In this long-time limit, the distribution for the number of $y \to z$ hops in time T behaves exactly like a Poisson point process [36]. The expected number of events, $\langle Tq(y,z)\rangle$, determines the rate of the asymptotically equivalent Poisson process. Consequently, the probability of observing empirical flow rate $q(y,z)$ in time T is asymptotically given by the Poisson distribution [28]:

$$P(q(y,z)) \asymp \frac{\langle Tq(y,z)\rangle^{-Tq(y,z)}\, e^{-\langle Tq(y,z)\rangle}}{(Tq(y,z))!}. \tag{14}$$

At long times, $\langle Tq(y,z)\rangle = p(y)r(y,z)$, so

$$P(p(y),q(y,z)) \asymp \frac{(p(y)r(y,z))^{-Tq(y,z)}\, e^{-p(y)r(y,z)}}{(Tq(y,z))!}. \tag{15}$$

This expression may be written in the large deviation form $P(p(y),q(y,z)) \asymp e^{-TI(p(y),q(y,z))}$ with the joint rate function

$$I(p(y),q(y,z)) = p(y)r(y,z) - q(y,z) + q(y,z)\ln\frac{q(y,z)}{p(y)r(y,z)}, \tag{16}$$

as in Eq. (8) of [20]. This result typically arises from more sophisticated arguments that construct an effective process to generate rare currents [20, 22]. While these arguments offer more rigor and alternative insight, we find our simple, heuristic derivation to be instructive since it clearly identifies the essential physics: we may discard temporal correlations in a complicated Markov jump process to obtain an asymptotically equivalent collection of Poisson point processes.

The same analysis applies to reversed transitions from mesostate z to y. Furthermore, correlations between $y \to z$ hops and $z \to y$ hops are also lost on sufficiently long timescales, so $q(y,z)$ and $q(z,y)$ are asymptotically independent with

$$P(p(y),p(z),q(y,z),q(z,y)) \asymp e^{-T\left[I\left(p(y),q(y,z)\right)+I\left(p(z),q(z,y)\right)\right]}. \tag{17}$$

Repeating this argument using all vertices and edges, gives $P(\boldsymbol{p},\boldsymbol{q}) \asymp e^{-TI(\boldsymbol{p},\boldsymbol{q})}$ with

$$I(\boldsymbol{p},\boldsymbol{q}) = \sum_{y\neq z} I(p(y),q(y,z)). \tag{18}$$

Finally, there is an important constraint for Markov jump processes that does not follow from simply analyzing the Poisson point processes. The Markov jump process allows transitions between mesostates but does not allow isolated birth or death events. Consequently, the jump process empirical flows conserve probability at every mesostate [37]:

$$\sum_z (q(y,z) - q(z,y)) = 0 \;\forall y. \tag{19}$$

Since the probability of a non-conservative empirical flow vanishes, we write $I(\boldsymbol{p},\boldsymbol{q}) = \infty$ when $\boldsymbol{q}$ does not satisfy Eq. (19).

Suppose now that we are interested in the empirical current across a single edge rather than the flow. Unlike $q(y,z)$, $j(y,z)$ deducts the rate of reversed hops from z to y. The probability of simultaneously recording a particular value of $p(y)$, $p(z)$, and $j(y,z)$ is thus given by marginalizing over the q's with the constraint $j(y,z) = q(y,z) - q(z,y)$. For large T, this marginalization proceeds via a saddle point approximation [27] to yield

$$P(p(y),p(z),j(y,z)) \asymp e^{-T\Psi(p(y),p(z),j(y,z))} \tag{20}$$

with

$$\Psi(p(y),p(z),j(y,z)) = \inf_{q(y,z)} I\Big(p(y),q(y,z)\Big) + I\Big(p(z),q(y,z)-j(y,z)\Big). \tag{21}$$

The minimizer $q_\star(y,z)$ is the root of a quadratic,

$$q_\star(y,z) = \frac{1}{2}\left(j(y,z) + \sqrt{j(y,z)^2 + a^p(y,z)^2}\right), \tag{22}$$

where $a^p(y,z) \equiv 2\sqrt{p(y)p(z)r(y,z)r(z,y)}$. The rate function Ψ may be expressed in terms of $q_\star$ as

$$\begin{aligned}\Psi(p(y),p(z),j(y,z)) &= I\big(p(y),q_\star(y,z)\big) + I\big(p(z),q_\star(z,y)\big)\\ &= \Big[p(y)r(y,z) + p(z)r(z,y) - q_\star(y,z) - q_\star(z,y)\\ &\quad + q_\star(y,z)\ln\frac{q_\star(y,z)}{p(y)r(y,z)} + q_\star(z,y)\ln\frac{q_\star(z,y)}{p(z)r(z,y)}\Big].\end{aligned} \tag{23}$$

In Appendix A we carry out straightforward algebraic manipulations to bring Ψ into the form of Bertini et al. [22],

$$\Psi = \sqrt{j^p(y,z)^2 + a^p(y,z)^2} - \sqrt{j(y,z)^2 + a^p(y,z)^2} + j(y,z)\left(\operatorname{arcsinh}\frac{j(y,z)}{a^p(y,z)} - \operatorname{arcsinh}\frac{j^p(y,z)}{a^p(y,z)}\right). \tag{24}$$

As in the case of the flows, joint fluctuations in all densities and currents follow by asymptotic independence, so $P(\boldsymbol{p},\boldsymbol{j}) \asymp e^{-TI(\boldsymbol{p},\boldsymbol{j})}$ with

$$I(\boldsymbol{p},\boldsymbol{j}) = \sum_{y<z} \Psi(p(y),p(z),j(y,z)). \tag{25}$$

Non-conservative empirical currents are disallowed in our dynamics, so we set $I(\boldsymbol{p},\boldsymbol{j}) = \infty$ if $\sum_z j(y,z) \neq 0$ for some y.

IV. RATE FUNCTION BOUND

To relate the fluctuations described by the rate function $I(\boldsymbol{p},\boldsymbol{j})$ to the thermodynamic dissipation, it is useful to write I in terms of the currents and thermodynamic forces $\boldsymbol{F}^p$. We first focus on Ψ. For notational compactness we suppress the labels of the vertices. We note that $j^p/\sinh(F^p/2) = a^p \geq 0$, implying that j^p has the same sign as F^p. Furthermore, it is natural to measure the empirical current j relative to the steady state current j^p, so we introduce $\bar{\jmath} \equiv j/j^p$. With this new notation,

$$\Psi = j^p\left[\coth\frac{F^p}{2} - \frac{\bar{\jmath}F^p}{2} + \bar{\jmath}\operatorname{arcsinh}\left(\bar{\jmath}\sinh\frac{F^p}{2}\right) - \sqrt{\bar{\jmath}^2 + \operatorname{csch}^2\frac{F^p}{2}}\right]. \tag{26}$$

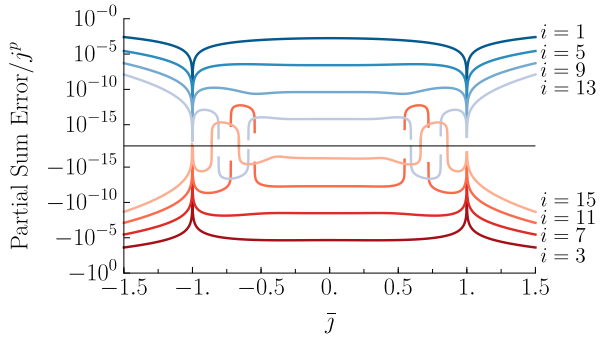

FIG. 3. Residuals from approximating Ψ by the partial sums of the Taylor series expansion in F^p, Eq. (27), plotted for $F^p = 0.75$. The label i indicates that the partial sum is computed up through (and including) the $(F^p)^i$ term in the series. The residual is this i^{th} partial sum minus Ψ. When $\bar{\jmath}$ is in the neighborhood of ± 1, the Taylor expansion for Ψ is an alternating series, so the partial sums provide upper and lower bounds on Ψ. For low-order partial sums and for small F^p the partial sums provide bounds for all values of $\bar{\jmath}$. As an example, the $i = 1$ partial sum is the quadratic bound given by Eq. (28), which holds for all values of $\bar{\jmath}$ and F^p.

Taylor expanding in powers of F^p, we obtain

$$\Psi = j^p\left[\frac{(\bar{\jmath}-1)^2F^p}{4} - \frac{(\bar{\jmath}^2-1)^2(F^p)^3}{192} + \frac{(\bar{\jmath}^2-1)^2(3\bar{\jmath}^2+1)(F^p)^5}{7680} + \mathcal{O}((F^p)^7)\right]. \tag{27}$$

The low-order partial sums of this series alternate, first over-estimating, then underestimating Ψ (see Fig. 3). In particular, the first partial sum bounds the rate function by a quadratic [24],

$$\Psi \le \Psi_{\text{quad}} \equiv \frac{(\bar{\jmath}-1)^2\sigma^p}{4}, \tag{28}$$

where $\sigma^p = j^pF^p$ is the local dissipation for the edge.

Truncation of a Taylor series, of course, does not necessarily yield a bound. To prove inequality (28) we must confirm the positivity of the residual $\Delta \equiv \Psi_{\text{quad}} - \Psi$. Since Δ is symmetric about $\bar{\jmath} = 0$, it suffices to consider positive $\bar{\jmath}$. We note that Δ vanishes when $\bar{\jmath} = 1$, and

$$\frac{\partial\Delta}{\partial\bar{\jmath}} = j^p\left[\operatorname{arcsinh}\left(\bar{\jmath}\sinh\frac{F^p}{2}\right) - \frac{\bar{\jmath}F^p}{2}\right], \tag{29}$$

implying that Δ strictly increases as $|\bar{\jmath}-1|$ grows [38]. Since $\Psi \le \Psi_{\text{quad}}$ is bounded for every edge of the graph, $I(\boldsymbol{p},\boldsymbol{j})$ is bounded by a quadratic form whose curvature is determined by the local entropy production rates:

$$I(\boldsymbol{p},\boldsymbol{j}) \le I_{\text{quad}}(\boldsymbol{p},\boldsymbol{j}) \equiv \sum_{y<z}\frac{\sigma^p(y,z)}{4j^p(y,z)^2}\left(j(y,z)-j^p(y,z)\right)^2, \tag{30}$$

Like $I(\boldsymbol{p},\boldsymbol{j})$, we demand that $I_{\text{quad}}(\boldsymbol{p},\boldsymbol{j})$ diverges when $\boldsymbol{j}$ is not a conservative current.

Recall that by construction $I(\boldsymbol{\pi},\boldsymbol{j}^\pi) = 0$. Our quadratic bound shares this minimum. Furthermore, $I(\boldsymbol{\pi},-\boldsymbol{j}^\pi) = I_{\text{quad}}(\boldsymbol{\pi},-\boldsymbol{j}^\pi)$, so I_{quad} is the tightest quadratic upper bound which has a minimum at $(\boldsymbol{\pi},\boldsymbol{j}^\pi)$ and is diagonal in the edge basis [25]. The curvature of I, evaluated at $\boldsymbol{\pi}$ and $\boldsymbol{j}^\pi$, reflects the variance of long-time current fluctuations. The tighter the inequality, (30), the more precisely we may relate this variance to the local entropy production rates. Truncation after the first-order term of the series expansion Eq. (27) becomes exact for small thermodynamic forces, meaning that the quadratic bound is accurate when F^p is small.

V. SCALAR CURRENT FLUCTUATIONS

The large deviation function $I(\boldsymbol{p},\boldsymbol{j})$ describes the joint distribution of density in all mesostates and currents between these states. Experiments, however, cannot hope to resolve the statistical details of a large number of degrees of freedom. To make practical use of inequality (30), we must project the result onto a smaller probability space. Rather than monitoring $\boldsymbol{p}$ and $\boldsymbol{j}$, suppose we only measure a scalar current of the form

$$j_d = \boldsymbol{j}\cdot\boldsymbol{d} \equiv \sum_{y<z} j(y,z)d(y,z). \tag{31}$$

The generalized current j_d is a linear combination of the currents between mesostates with expansion coefficients $\boldsymbol{d}$ [23]. This construction affords significant flexibility. By choosing $\boldsymbol{d} = \boldsymbol{F}^\pi$, the generalized current is the same as the dissipation rate. Other choices of $\boldsymbol{d}$ can highlight the current across a single edge or the current associated with transitions between macrostates, as illustrated in Section VII.

In the long-time limit, the distribution for this generalized current adopts the large deviation form $P(j_d) \asymp e^{-TI(j_d)}$. Because $P(j_d)$ can be constructed from $P(\boldsymbol{p},\boldsymbol{j})$ by marginalization, the rate function for the generalized current is related to $I(\boldsymbol{p},\boldsymbol{j})$ [39]:

$$I(j_d) = \inf_{\boldsymbol{p},\boldsymbol{j}|\boldsymbol{j}\cdot\boldsymbol{d}=j_d} I(\boldsymbol{p},\boldsymbol{j}). \tag{32}$$

The infimum is bounded from above by $I(\boldsymbol{p}^*,\boldsymbol{j}^*)$ for any choice of $\boldsymbol{p}^*$ and conservative $\boldsymbol{j}^*$ such that $\boldsymbol{j}^*\cdot\boldsymbol{d} = j_d$. We choose $\boldsymbol{p}^* = \boldsymbol{\pi}$ and $\boldsymbol{j}^* = (j_d/j_d^\pi)\boldsymbol{j}^\pi$, where $j_d^\pi \equiv \boldsymbol{j}^\pi\cdot\boldsymbol{d}$. As a multiple of the conservative steady state current $\boldsymbol{j}^\pi$, $\boldsymbol{j}^*$ is guaranteed to be conservative. Hence

$$\begin{aligned} I(j_d) &\le I(\boldsymbol{p}^*,\boldsymbol{j}^*) \\ &= \frac{1}{4}\left(\frac{j_d}{j_d^\pi}-1\right)^2\sum_{y<z}\sigma^\pi(y,z) \\ &= \frac{(j_d-j_d^\pi)^2\Sigma^\pi}{4(j_d^\pi)^2}, \end{aligned} \tag{33}$$

where we have used inequality (30). The bound on the large deviation function translates to a bound on the variance of j_d since $\mathrm{var}(j_d) = 1/I''(j_d^\pi)$. Measuring the mean and variance of any scalar current provides a lower bound on the dissipation rate:

$$\frac{2(j_d^\pi)^2}{\mathrm{var}(j_d)} \leq \Sigma^\pi. \tag{34}$$

The bound on Σ^π is most useful if it is tight, but there are two distinct reasons it might be loose: (1) Ψ for the edges could deviate significantly from the quadratic bound Ψ_{quad} or (2) our choice of $\boldsymbol{p}^*$ and $\boldsymbol{j}^*$ could be suboptimal. In the remainder of the paper we study diffusion processes as a limit of Markov jump processes. That limiting procedure yields $\Psi = \Psi_{\mathrm{quad}}$, so the diffusion process bound is weakened only by our suboptimal $\boldsymbol{p}^*$ and $\boldsymbol{j}^*$. Thus for diffusions, the high-dimensional rate function $I(\boldsymbol{p}, \boldsymbol{j})$ is exactly given by the quadratic $I_{\mathrm{quad}}(\boldsymbol{p}, \boldsymbol{j})$, but the low-dimensional rate function $I(j_d)$ can still differ significantly from the upper bound in inequality (33). Section VII considers this scenario in greater detail.

VI. DIFFUSION PROCESSES

Though our results have been derived for Markov jump processes, we may translate them into appropriate forms to describe fluctuations in diffusion processes. For simplicity, we consider the motion of a particle in two dimensions with mobility μ. Let $\boldsymbol{x} \equiv (x_1, x_2)$ denote the particle's position, which evolves according to an overdamped Langevin equation with deterministic force $\boldsymbol{f}(\boldsymbol{x}) \equiv (f_1(\boldsymbol{x}), f_2(\boldsymbol{x}))$ and random force η. We further decompose the deterministic force into a contribution from an free energy gradient $\nabla U(\boldsymbol{x})$ and one from a non-gradient external field $\boldsymbol{f}_{\mathrm{ext}}(\boldsymbol{x})$,

$$\frac{\partial \boldsymbol{x}}{\partial t} = -\mu \nabla U(\boldsymbol{x}) + \mu \boldsymbol{f}_{\mathrm{ext}}(\boldsymbol{x}) + \boldsymbol{\eta}. \tag{35}$$

The random force at time t, $\boldsymbol{\eta}(t) \equiv (\eta_1(t), \eta_2(t))$ is a vector of Gaussian random variables satisfying $\langle \eta_k(t) \rangle = 0$ and $\langle \eta_k(t) \eta_{k'}(t') \rangle = 2D\delta_{k,k'}\delta(t-t')$, where D is the diffusion constant. In Section VII we will consider the particular driven diffusive process shown in Fig. 4 as an illustrative example.

Associated to the Langevin equation is a Fokker-Planck equation describing the evolution of probability density at position $\boldsymbol{x}$, $\rho(\boldsymbol{x})$:

$$\frac{\partial \rho(\boldsymbol{x})}{\partial t} = -\nabla \cdot \boldsymbol{\mathcal{J}}^\rho(\boldsymbol{x}), \tag{36}$$

where

$$\boldsymbol{\mathcal{J}}^\rho(\boldsymbol{x}) \equiv (\mathcal{J}_1^\rho(\boldsymbol{x}), \mathcal{J}_2^\rho(\boldsymbol{x})) = \boldsymbol{f}(\boldsymbol{x})\rho(\boldsymbol{x}) - D\nabla\rho(\boldsymbol{x}) \tag{37}$$

is the ρ-dependent current at $\boldsymbol{x}$. We denote the steady-state density ρ^π and the steady-state current $\boldsymbol{\mathcal{J}}^\pi$. As

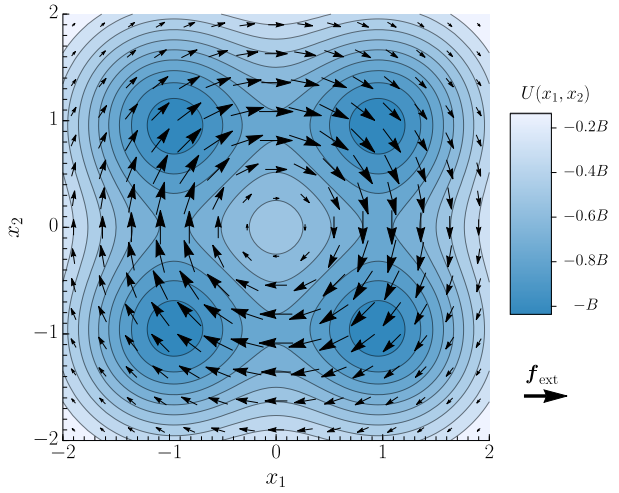

FIG. 4. Contour plot of a free energy $U(\boldsymbol{x}) = -B\sum_{i=1}^4 e^{-(\boldsymbol{x}-\boldsymbol{c}_i)^2}$, with the $\boldsymbol{c}_i$'s setting the center of the Gaussian wells at $(\pm 1, \pm 1)$. The parameter B controls the barrier heights (or equivalently the well depths). The black arrows represent a vector field of the non-gradient external field, $\boldsymbol{f}_{\mathrm{ext}}(\boldsymbol{x}) = A\boldsymbol{x}^2 e^{-3|\boldsymbol{x}|}(x_2, -x_1)$, which drives cycles around the origin. The external field's amplitude is regulated by the parameter $A = 8$.

in the jump process, we define an empirical density field and empirical current field, ρ and $\boldsymbol{\mathcal{J}}$ respectively, and measure the probability of fluctuations away from ρ^π and $\boldsymbol{\mathcal{J}}^\pi$ using the rate function $\mathcal{I}[\rho, \boldsymbol{\mathcal{J}}]$. The square brackets highlight that $\mathcal{I}$ is now a functional of the density and current fields. The exact form of $\mathcal{I}$ is known [25, 40]. In this section, we give a new derivation of the result using a limit of the Markov jump process results. The limiting procedure serves to clarify the origin of quadratic current fluctuations in diffusion processes.

To leverage our previous results, we approximate the diffusion process by a jump process on a square lattice, as depicted in Fig. 5. There is no unique way to coarse-grain a diffusion to a jump process [41]. Thus we have freedom in how we construct our model so long as it yields a diffusive limit that matches the Fokker-Planck equation, Eq. (36), when the lattice spacing becomes infinitesimal. We construct a simple nearest-neighbor jump process which is entirely characterized by four space-dependent transition rates for hopping from a grid point at $\boldsymbol{x}$ to a nearest-neighbor site: $W_{\mathrm{up}}(\boldsymbol{x}), W_{\mathrm{right}}(\boldsymbol{x}), W_{\mathrm{down}}(\boldsymbol{x})$, and $W_{\mathrm{left}}(\boldsymbol{x})$. These rates must scale with the lattice spacing h in such a way that the first two jump moments give the correct drift and diffusion [41], requiring

$$\begin{aligned} h(W_{\mathrm{right}}(\boldsymbol{x}) - W_{\mathrm{left}}(\boldsymbol{x})) &= \mu f_1(\boldsymbol{x}) \\ h(W_{\mathrm{up}}(\boldsymbol{x}) - W_{\mathrm{down}}(\boldsymbol{x})) &= \mu f_2(\boldsymbol{x}) \\ h^2(W_{\mathrm{right}}(\boldsymbol{x}) + W_{\mathrm{left}}(\boldsymbol{x})) &= 2D \\ h^2(W_{\mathrm{up}}(\boldsymbol{x}) + W_{\mathrm{down}}(\boldsymbol{x})) &= 2D. \end{aligned} \tag{38}$$

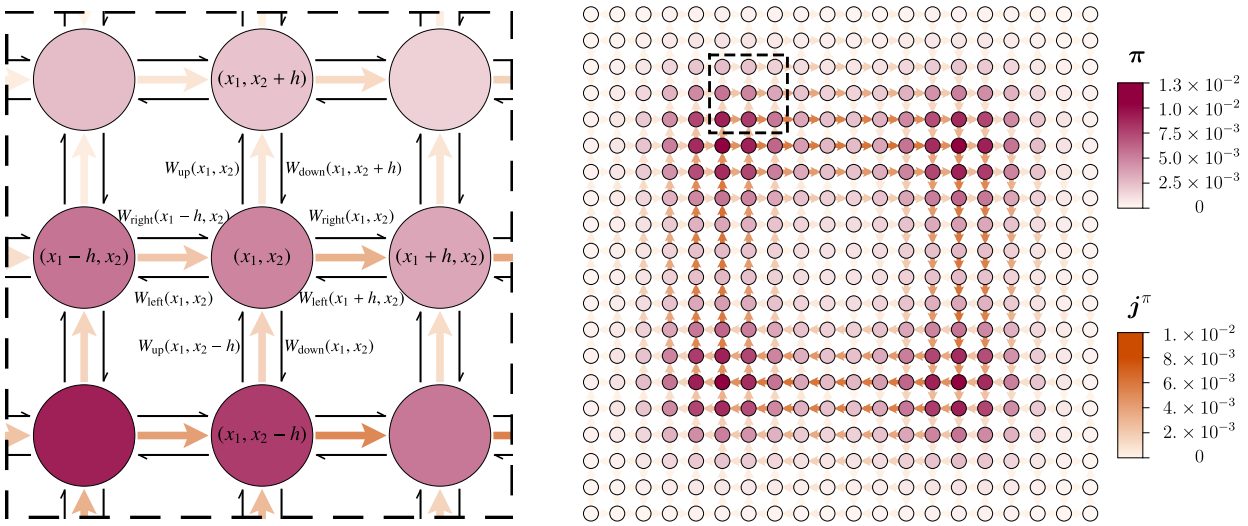

FIG. 5. Jump process approximating the diffusion in Fig. 4. On the left, a close-up view of a sub-system shows the transition rates on the lattice. On the right, the steady state behavior of the full state space ($\boldsymbol{x} \in [-2, 2] \times [-2, 2]$) is shown for $A = 8, B = 5, D = 1, \mu = 1$. The steady-state density primarily resides in the four wells, but the external field drives some clockwise current around the origin.

From these constraints the hopping rates are

$$\begin{aligned} W_{\text{right}}(\boldsymbol{x}) &= \frac{\mu f_1(\boldsymbol{x})}{2h} + \frac{D}{h^2} \\ W_{\text{left}}(\boldsymbol{x}) &= \frac{-\mu f_1(\boldsymbol{x})}{2h} + \frac{D}{h^2} \\ W_{\text{up}}(\boldsymbol{x}) &= \frac{\mu f_2(\boldsymbol{x})}{2h} + \frac{D}{h^2} \\ W_{\text{down}}(\boldsymbol{x}) &= \frac{-\mu f_2(\boldsymbol{x})}{2h} + \frac{D}{h^2}. \end{aligned} \tag{39}$$

We now identify each vertex of the graph by its location $\boldsymbol{x}$, writing the density at that vertex as $p(\boldsymbol{x})$. The edge connecting grid point $\boldsymbol{x}$ to its neighbor on the right has current $j^p_{\text{right}}(\boldsymbol{x}) \equiv j^p(\boldsymbol{x}, \boldsymbol{x} + (h, 0))$, and the thermodynamic force associated to that edge is $F^p_{\text{right}}(\boldsymbol{x}) \equiv F^p(\boldsymbol{x}, \boldsymbol{x} + (h, 0))$. The "up," "down," and "left" directions are treated analogously. Using this notation, we may rewrite I_{quad} of Eq. (30) as

$$\begin{aligned} I_{\text{quad}}(\boldsymbol{p}, \boldsymbol{j}) = \frac{1}{8} \sum_{\boldsymbol{x}} \Bigg[& \frac{F^p_{\text{left}}(\boldsymbol{x})}{j^p_{\text{left}}(\boldsymbol{x})} (j_{\text{left}}(\boldsymbol{x}) - j^p_{\text{left}}(\boldsymbol{x}))^2 \\ & + \frac{F^p_{\text{right}}(\boldsymbol{x})}{j^p_{\text{right}}(\boldsymbol{x})} (j_{\text{right}}(\boldsymbol{x}) - j^p_{\text{right}}(\boldsymbol{x}))^2 \\ & + \frac{F^p_{\text{down}}(\boldsymbol{x})}{j^p_{\text{down}}(\boldsymbol{x})} (j_{\text{down}}(\boldsymbol{x}) - j^p_{\text{down}}(\boldsymbol{x}))^2 \\ & + \frac{F^p_{\text{up}}(\boldsymbol{x})}{j^p_{\text{up}}(\boldsymbol{x})} (j_{\text{up}}(\boldsymbol{x}) - j^p_{\text{up}}(\boldsymbol{x}))^2 \Bigg]. \end{aligned} \tag{40}$$

To simplify the expression further, we must convert from the discrete-space density $\boldsymbol{p}$ and current $\boldsymbol{j}$ to the fields ρ and $\boldsymbol{\mathcal{J}}$. In the continuum limit, $\boldsymbol{p}(\boldsymbol{x})$ vanishes while $\rho(\boldsymbol{x})$ remains finite such that $\boldsymbol{p}(\boldsymbol{x}) \to h^2 \rho(\boldsymbol{x})$. The current field $\boldsymbol{\mathcal{J}}^\rho$ is also finite, but the current on any edge of the lattice vanishes with order h:

$$\begin{aligned} j^p_{\text{right}}(\boldsymbol{x}) &= p(\boldsymbol{x}) W_{\text{right}}(\boldsymbol{x}) - p\Big(\boldsymbol{x} + (h, 0)\Big) W_{\text{left}}\Big(\boldsymbol{x} + (h, 0)\Big) \\ &= \left(\mu f_1(\boldsymbol{x}) \rho(\boldsymbol{x}) - D \frac{\partial \rho(\boldsymbol{x})}{\partial x_1} \right) h + \mathcal{O}(h^2) \\ &= \mathcal{J}^\rho_1(\boldsymbol{x}) h + \mathcal{O}(h^2). \end{aligned} \tag{41}$$

Likewise, the thermodynamic force on each edge vanishes in proportion to h:

$$\begin{aligned} F^p_{\text{right}}(\boldsymbol{x}) &= \ln \frac{p(\boldsymbol{x}) W_{\text{right}}(\boldsymbol{x})}{p\Big(\boldsymbol{x} + (h, 0)\Big) W_{\text{left}}\Big(\boldsymbol{x} + (h, 0)\Big)} \\ &= \left(\frac{\mu f_1(\boldsymbol{x})}{D} - \frac{1}{p(\boldsymbol{x})} \frac{\partial p(\boldsymbol{x})}{\partial x_1} \right) h + \mathcal{O}(h^2) \\ &= \mathcal{F}^\rho_1(\boldsymbol{x}) h + \mathcal{O}(h^2), \end{aligned} \tag{42}$$

with a finite thermodynamic force field given by

$$\boldsymbol{\mathcal{F}}^\rho(\boldsymbol{x}) \equiv (\mathcal{F}^\rho_1(\boldsymbol{x}), \mathcal{F}^\rho_2(\boldsymbol{x})) = \frac{\mu \boldsymbol{f}(\boldsymbol{x})}{D} - \nabla \ln \rho(\boldsymbol{x}). \tag{43}$$

Hence the ratio of force to current on an edge, which appears in each term of Eq. (40), remains finite and independent of the jump direction,

$$\lim_{h \to 0} \frac{F^p_{\text{right}}(\boldsymbol{x})}{j^p_{\text{right}}(\boldsymbol{x})} = \frac{\mathcal{F}^\rho_1(\boldsymbol{x})}{\mathcal{J}^\rho_1(\boldsymbol{x})} = \frac{\frac{\mu f_1}{D} - \frac{\partial}{\partial x_1} \ln \rho(\boldsymbol{x})}{\mu f_1 \rho - D \frac{\partial}{\partial x_1} \rho(\boldsymbol{x})} = \frac{1}{D \rho(\boldsymbol{x})}. \tag{44}$$

Recall from Eq. (27) that the rate function bound (30) becomes tighter for small thermodynamic forces. Since the forces vanish in the $h \to 0$ limit, the jump process on an infinitesimal grid thus saturates inequality (30), yielding the equality

$$\mathcal{I}[\rho, \boldsymbol{\mathcal{J}}] = \lim_{h\to 0} I(\boldsymbol{p}, \boldsymbol{j}) = \lim_{h\to 0} I_{\text{quad}}(\boldsymbol{p}, \boldsymbol{j}). \tag{45}$$

In other words, approximating I by I_{quad} becomes exact in the continuum limit. We convert the sum to an integral,

$$\sum_{\boldsymbol{x}} h^2 \to \int d\boldsymbol{x}, \tag{46}$$

and insert Eqs. (41) and (44) into Eq. (40) to obtain the rate function for diffusions

$$\mathcal{I}[\rho, \boldsymbol{\mathcal{J}}] = \int d\boldsymbol{x} \frac{(\boldsymbol{\mathcal{J}}(\boldsymbol{x}) - \boldsymbol{\mathcal{J}}^{\rho}(\boldsymbol{x}))^2}{4D\rho(\boldsymbol{x})}. \tag{47}$$

Note that the current fluctuations are strictly quadratic, a fact that can be traced back to the vanishingly small thermodynamic force on each infinitesimal edge of the graph.

The rate function may alternatively be expressed with respect to the local dissipation rates,

$$\boldsymbol{\sigma}^{\rho}(\boldsymbol{x}) = \boldsymbol{\mathcal{J}}^{\rho}(\boldsymbol{x}) \cdot \boldsymbol{\mathcal{F}}^{\rho}(\boldsymbol{x}) = \frac{\boldsymbol{\mathcal{J}}^{\rho}(\boldsymbol{x})^2}{D\rho(\boldsymbol{x})}. \tag{48}$$

Interpreting $\boldsymbol{\sigma}^{\rho}$ as a physical dissipation requires that the particle exchanges energy with a thermal reservoir at inverse temperature β and satisfies the Einstein relation $\beta D = \mu$. The second equality follows from a rearrangement of Eq. (44),

$$\boldsymbol{\mathcal{J}}^{\rho}(\boldsymbol{x}) = D\boldsymbol{\mathcal{F}}^{\rho}(\boldsymbol{x})\rho(\boldsymbol{x}), \tag{49}$$

which is an expression of linear response; the current at any point in space is linearly proportional to the thermodynamic force at that point. Finally, we obtain a form for $\mathcal{I}$ analogous to the right-hand side of inequality (30), but for diffusion processes the inequality has become an equality. This shows that the current fluctuations are specified by local dissipation rates:

$$\mathcal{I}[\rho, \boldsymbol{\mathcal{J}}] = \int d\boldsymbol{x} \, \frac{\boldsymbol{\sigma}^{\rho}(\boldsymbol{x})}{4\boldsymbol{\mathcal{J}}^{\rho}(\boldsymbol{x})^2} \left(\boldsymbol{\mathcal{J}}(\boldsymbol{x}) - \boldsymbol{\mathcal{J}}^{\rho}(\boldsymbol{x})\right)^2. \tag{50}$$

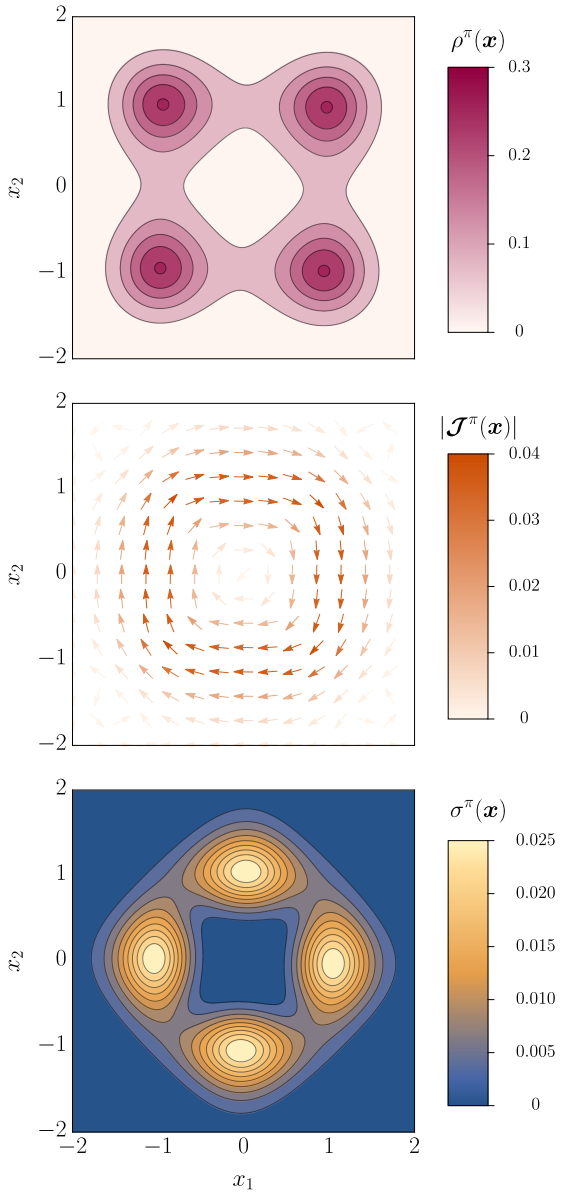

FIG. 6. Steady-state density field, current field, and local dissipation rate (top to bottom) for the example from Fig. 4 with $A = 8, B = 5, D = 1, \mu = 1$. The diffusion process was approximated by a jump process on a 400 x 400 grid, and the master equation was solved in discrete space. Note that the local dissipation rate is largest at the barriers, where the density is low and the current high.

VII. COARSE-GRAINING IN SPACE

Up to this point we have assumed a mesoscopic Markov process that is monitored with complete precision. More commonly, it is only possible to observe coarse-grained macrostates, and transitions between them are not be Markovian. Rather, the macroscopic dynamics is described by a hidden Markov model [42]. Remarkably, current fluctuations in the non-Markovian macroscopic dynamics carry information about the dissipation rate of the underlying mesoscopic degrees of freedom.

To demonstrate the connection between dissipation and a macroscopic current, we measure the generalized scalar current j_d, defined in Eq. (31). The vector $\boldsymbol{d}$ determines which microscopic transitions are observable, so for a suitable choice of $\boldsymbol{d}$, j_d is the macroscopic current. Consider, for example, the two-dimensional driven diffu-

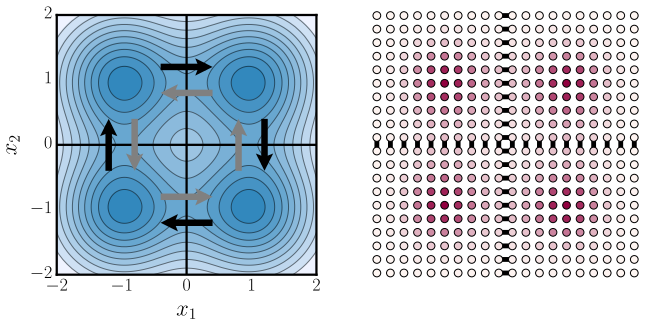

FIG. 7. Left: The driven diffusion process in Fig. 4 is naturally coarse-grained into four states, and the macroscopic current is constructed by monitoring transitions between them. Clockwise transitions (black arrows) are given the weight +1 while counterclockwise transitions (gray arrows) carry weight −1. All motion within a coarse-grained macrostate is undetected. Right: In practice, we compute large deviation properties of the coarse-grained current by solving the diffusion process on a grid, as in Sec. VI. On the grid, j_d is constructed by weighting the black edges by ±1 and all other edges by 0 as specified in Eq. (53).

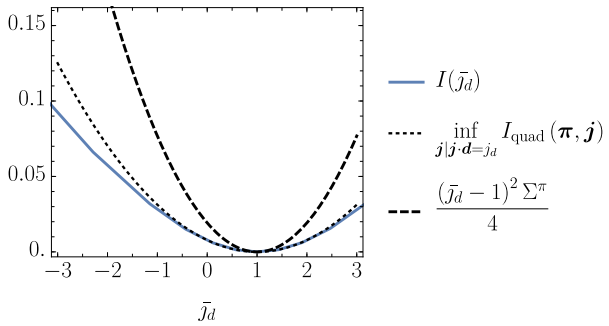

FIG. 8. Large deviation function for the macroscopic current with the four coarse-grained states in Fig. 7. U and $\boldsymbol{f}_{\text{ext}}$ are given by Eqs. (51) and (52), respectively, with $A = 8, B = 5$. Macroscopic currents are expressed in relation to the steady state value: $\bar{j}_d \equiv j_d/j_d^\pi$. The blue line shows the current fluctuations for the diffusion process solved on a grid of 400 x 400 states. $I(j_d)$ is the numerical Legendre transform of a scaled cumulant generating function, computed as the maximum eigenvalue of a tilted rate matrix [27, 43, 44]. The dotted black line is the result of the constrained minimization of the quadratic form, computed as described in Appendix B. This constrained minimization very closely approximates $I(\bar{j}_d)$ for small deviations. The dashed black line is the quadratic rate function bound Eq. (33) with curvature regulated by the total dissipation rate.

sion process in Fig. 4. A particle evolves on a free energy landscape

$$U(\boldsymbol{x}) = -B\sum_{i=1}^{4} e^{-(\boldsymbol{x}-\boldsymbol{c}_i)^2} \tag{51}$$

with B controlling the depth of four Gaussian wells centered at $\boldsymbol{c} = (\pm 1, \pm 1)$. At a coarse-grained level, these wells define four possible macrostates. In addition to the free energy landscape, we introduce a non-gradient external field with amplitude A,

$$\boldsymbol{f}_{\text{ext}}(\boldsymbol{x}) = A\boldsymbol{x}^2 e^{-3|\boldsymbol{x}|}(x_2, -x_1), \tag{52}$$

which drives transitions between the macrostates. The macroscopic current is the rate of clockwise (CW) transitions between these coarse-grained states less the rate of counter-clockwise (CCW) transitions. As illustrated in Fig. 7, we measure this current, $j_d = \boldsymbol{j}\cdot\boldsymbol{d}$, by choosing

$$d(y,z) = \begin{cases} 1, & y \to z \text{ a CW macrostate transition} \\ -1, & y \to z \text{ a CCW macrostate transition} \\ 0, & \text{otherwise.} \end{cases} \tag{53}$$

The results from Sec. V directly apply to this construction. In particular, inequality (34) implies $\Sigma^\pi \geq 2(j_d^\pi)^2/\text{var}(j_d)$. The right-hand side of this inequality depends on the first two moments of the *macroscopic* empirical current distribution. By measuring these moments with coarse-grained observations, we therefore bound the total entropy production of the *mesoscopic* system, Σ^π.

To assess the inequality's tightness, we used a 400 x 400 grid to numerically compute $I(j_d)$ for the four-well model with $D = \mu = 1$, and with various choices of A and B. We saw in Sec. VI that I_{quad} becomes exact in the diffusive limit, so

$$I(j_d) = \inf_{\boldsymbol{p},\boldsymbol{j}|\boldsymbol{j}\cdot\boldsymbol{d}=j_d} I_{\text{quad}}(\boldsymbol{p},\boldsymbol{j}) \leq \inf_{\boldsymbol{j}|\boldsymbol{j}\cdot\boldsymbol{d}=j_d} I_{\text{quad}}(\boldsymbol{\pi},\boldsymbol{j}). \tag{54}$$

The numerical results, plotted in Fig. 8, reflect that inequality (54) is a tight bound. In contrast, the dissipation rate bound, inequality (33), is noticeably weaker. A measure of this weakness is the ratio

$$\phi = \left(\frac{2(j_d^\pi)^2}{\text{var}(j_d)}\right)/\Sigma^\pi, \tag{55}$$

which ranges from 0 to 1. This ratio, plotted in Fig. 9 for a range of driving amplitudes and well depths, assesses the fraction of the dissipation rate that can be inferred from the macroscopic current fluctuations.

It has been shown that our inference strategy detects the greatest fraction of dissipation if the macroscopic current is constructed to be proportional to the thermodynamic force [24]. More precisely, $\phi = 1$ when $\boldsymbol{d} \propto \boldsymbol{F}^\pi$, and ϕ decreases when the vector $\boldsymbol{d}$ is less aligned with $\boldsymbol{F}^\pi$. In our coarse-graining set-up, the elements of $\boldsymbol{d}$ are set to 0 or ±1 based on whether each mesoscopic transition is observable. With this $\boldsymbol{d}$ by the constraints of what transitions are observable, ϕ can only be varied by altering A and B to change $\boldsymbol{F}^\pi$.

We can understand ϕ's dependence on these model parameters by analyzing the degree to which $\boldsymbol{F}^\pi$ aligns with $\boldsymbol{d}$. Fig. 10 illustrates how the continuous thermodynamic

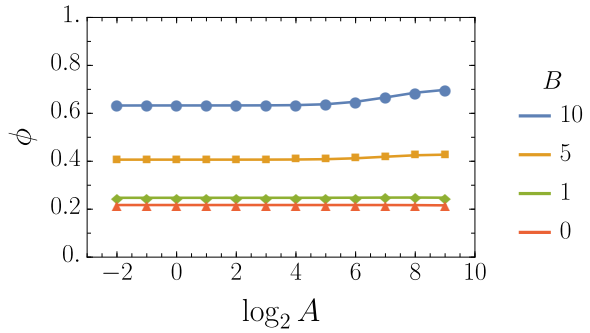

FIG. 9. Fraction of the total dissipation rate which can be deduced from the macroscopic current fluctuations in the four-well diffusion model defined by Eqs. (51) and (52). A controls the amplitude of the external driving field and B controls the well depths. Equation (55) defines ϕ, which takes the value 1 when the current fluctuations account for all of the dissipation. Values of ϕ were computed by representing the diffusion process as a jump process on a 400×400 grid. For large B, the wells become deep metastable states which are amenable to coarse-graining, so the macroscopic current accounts for a significant fraction of the dissipation.

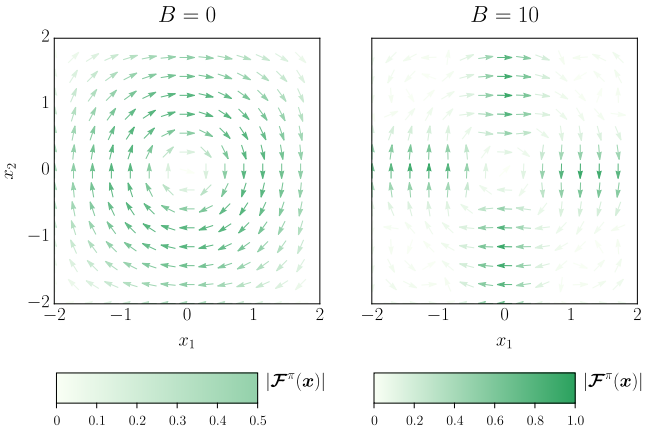

FIG. 10. Thermodynamic force for the four-well model with $A = 8$, solved on a 400×400 grid. For large B, the free energy landscape has deep wells, and the thermodynamic forces are large along the barriers separating the wells. In this large-B limit, the thermodynamic force resembles $\boldsymbol{d}$, which vanishes everywhere except for along the axes.

force field $\boldsymbol{\mathcal{F}}^\pi(\boldsymbol{x})$ varies with the well depth. In the absence of wells ($B = 0$), the thermodynamic force is radially symmetric about the origin. As the wells are made deeper, $\boldsymbol{\mathcal{F}}^\pi$ is amplified along the axes, more closely resembling $\boldsymbol{d}$ of Fig. 7. This resemblance explains the trend that ϕ increases with increasing B. Interestingly, ϕ depends only weakly on the external field amplitude, a fact we rationalize with a linear-response argument at the end of Appendix B.

VIII. CONCLUSIONS

It is typically impossible to resolve detailed mesoscopic dynamics, even with the most sophisticated experimental tools. Because the dissipation rate is defined in terms of such immeasurable mesoscopic transitions, it may seem that there is no hope of experimentally measuring the dissipation, short of explicitly detecting the free energetic flows from the thermodynamic reservoirs. Our models and analysis demonstrate that, in fact, a bound on the total dissipation can be inferred by monitoring only the fluctuations in macroscopic currents. The procedure we use to infer this bound is extremely adaptable; we make essentially no assumptions about the mesoscopic details of the system nor about the macroscopic currents that will be observed.

Crucially, it is the macroscopic current fluctuations, not their averages, that reveal the dissipation of the unobserved mesoscopic dynamics. Motivated by the inability to fully resolve mesoscopic dynamics in an experiment, we have constructed a coarse-grained macroscopic current by recording a small subset of the mesoscopic transitions. The fraction of total dissipation due to one of these observed transitions is small, and in fact vanishes in the diffusive limit. Were we to measure only the average current through the observed links, we would at best deduce this infinitesimally small portion of the total dissipation. However, if we use the fluctuation dissipation relation for the observed currents, we tacitly constrain the average behavior of all the unobserved transitions. Hence the fluctuations in a tiny subset of the mesoscopic transitions carry information about an appreciable fraction of the total dissipation. This useful fact stems from a fundamental bound on the extent of fluctuations: the total dissipation rate sets a bound for the variance in *any* generalized current.

We anticipate that our inference scheme will be a robust strategy for analyzing dissipation in stochastic, biophysical systems. The extent to which coarse-grained fluctuations reveal the total dissipation, measured by ϕ, depends on the fidelity of the coarse-graining. For the model we studied in Sec. VII, ϕ nears 1 when the wells are sufficiently deep that the coarse-grained states are long-lived metastable macrostates. The step-like dynamics of dissipative biological machines [45, 46] demonstrate precisely this type of metastability. Indeed, it is often the goal of biological studies to assign the experimentally observed metastable macrostates to coarse-grained descriptions, e.g., ligation states. Together, these observations bolster the prospect of accurately inferring dissipation rates using data from single molecule experiments.

ACKNOWLEDGMENTS

This research is funded by the Gordon and Betty Moore Foundation to TRG as a Physics of Living Systems Fellow through Grant GBMF4513 and to JMH through

Grant GBMF4343. GMR was supported by a National Science Foundation Graduate Research Fellowship.

Appendix A: Derivation of equivalent forms of Ψ

In the main text we have extensively discussed the time-asymmetric empirical current from state y to z, $j(y,z)$. This quantity is time-asymmetric because it acquires a negative sign if the trajectory is run backwards in time. Maes and coworkers have highlighted the importance of the time-symmetric empirical traffic, which counts the total number of hops across the yz edge in either direction [12, 20, 47–49]. As in our study of the currents, we monitor two different forms of the traffic: the expected traffic given $\boldsymbol{p}$, $t^p(y,z) = p(y)r(y,z) + p(z)r(z,y)$, and the traffic $t_\star(y,z) = q_\star(y,z) + q_\star(z,y)$. Ψ naturally decomposes into contributions from the traffic and contributions from the currents, $\Psi = \Psi_{\text{traffic}} + \Psi_{\text{current}}$ [20], with

$$\Psi_{\text{traffic}} \equiv p(y)r(y,z) + p(z)r(z,y) - q_\star(y,z) - q_\star(z,y)$$

and

$$\Psi_{\text{current}} \equiv q_\star(y,z)\ln\frac{q_\star(y,z)}{p(y)r(y,z)} + q_\star(z,y)\ln\frac{q_\star(z,y)}{p(z)r(z,y)}. \tag{A1}$$

Ψ_{traffic} is simply the difference between the expected and the observed number of hops, $\Psi_{\text{traffic}} = t^p(y,z) - t_\star(y,z)$. To bring Ψ_{traffic} into the form that appears in Eq. (24), we recognize that $t_\star(y,z) = \sqrt{j(y,z)^2 + a^p(y,z)^2}$ and that $t^p(y,z) = \sqrt{j^p(y,z)^2 + a^p(y,z)^2}$. Simplifying Ψ_{current} is slightly more involved. Using the solution for $q_\star$, Eq. (22), Ψ_{current} can be rewritten in the form of Eq. (24),

$$\begin{aligned}
\Psi_{\text{current}} &= \frac{j(y,z)}{2}\ln\frac{q_\star(y,z)p(z)r(z,y)}{q_\star(z,y)p(y)r(y,z)} \\
&\quad + \frac{\sqrt{j(y,z)^2 + a^p(y,z)^2}}{2}\underbrace{\ln\frac{q_\star(y,z)q_\star(z,y)}{p(y)r(y,z)p(z)r(z,y)}}_{0} \\
&= \frac{j(y,z)}{2}\left(\ln\frac{q_\star(y,z)}{q_\star(z,y)} + \ln\frac{p(z)r(z,y)}{p(y)r(y,z)}\right) \\
&= \frac{j(y,z)}{2}\ln\frac{j(y,z) + \sqrt{j(y,z)^2 + a^p(y,z)^2}}{-j(y,z) + \sqrt{j(y,z)^2 + a^p(y,z)^2}} \\
&\quad + \frac{j(y,z)}{2}\ln\frac{j^p(y,z) + \sqrt{j^p(y,z)^2 + a^p(y,z)^2}}{-j^p(y,z) + \sqrt{j^p(y,z)^2 + a^p(y,z)^2}} \\
&= j(y,z)\left(\operatorname{arcsinh}\frac{j(y,z)}{a^p(y,z)} - \operatorname{arcsinh}\frac{j^p(y,z)}{a^p(y,z)}\right).
\end{aligned} \tag{A2}$$

Appendix B: Tight Quadratic Current Fluctuation Bound

In the main text, an upper bound for $I(j_d)$ was obtained by guessing $\boldsymbol{p}^* = \boldsymbol{\pi}$ and $\boldsymbol{j}^* = (j_d/j_d^\pi)\boldsymbol{j}^\pi$. This guess implies that the chance of measuring a value j_d is at least as likely as it would be if we simultaneously scaled all of the steady-state mesoscopic currents so as to make $\boldsymbol{j}^* \cdot \boldsymbol{d} = j_d$. There can, however, be more likely ways to obtain j_d which do not equally scale the different mesoscopic currents. Identifying the optimum is a straightforward exercise in linear algebra: the quadratic form I_{quad} must be extremized subject to the linear constraint $\boldsymbol{j} \cdot \boldsymbol{d} = j_d$ and to current conservation. The restriction to conservative currents may be imposed by a collection of Lagrange multipliers, one per node, as in Ref. [24] or by expressing the currents in a cycle basis as in Ref. [25, 50]. We use the second strategy here. Since both strategies exactly solve the same convex optimization problem, they must yield the same solution.

Let $a(i)$ be the current around the i^{th} cycle in a complete cycle basis. This basis may be constructed from spanning trees [51], but for now the particular cycle basis is immaterial. We introduce

$$\chi^i_{yz} = \begin{cases} 1, & \text{cycle } i \text{ contains edge } yz \text{ with } y < z \\ -1, & \text{cycle } i \text{ contains edge } yz \text{ with } z < y \\ 0, & \text{otherwise} \end{cases} \tag{B1}$$

to convert between the edge basis and the cycle basis so that

$$j(y,z) = \sum_i \chi^i_{yz} a(i). \tag{B2}$$

Recall that

$$I_{\text{quad}}(\boldsymbol{p},\boldsymbol{j}) = \begin{cases} \sum_{y<z} \frac{\sigma^p(y,z)}{4}\left(\frac{j(y,z)}{j^p(y,z)} - 1\right)^2, & \text{conservative } \boldsymbol{j} \\ \infty, & \text{otherwise.} \end{cases} \tag{B3}$$

In terms of the cycle basis the restriction to conservative currents is more natural:

$$\begin{aligned}
I_{\text{quad}}(\boldsymbol{p},\boldsymbol{a}) &= \sum_{y<z}\left(\sum_i \chi^i_{yz}(a(i) - a^p(i))\right)^2 \frac{F^p(y,z)}{4j^p(y,z)} \\
&= \frac{1}{2}\sum_{i,k}(a(i) - a^p(i))G_{ik}(a(k) - a^p(k)),
\end{aligned} \tag{B4}$$

with $G_{ik} = \sum_{y<z}\chi^i_{yz}\chi^k_{yz}\frac{F^p(y,z)}{2j^p(y,z)}$ [25]. We also translate the linear constraint into the cycle basis:

$$j_d = \sum_{y<z}\sum_i \chi^i_{yz}a(i)d(y,z) = \sum_i a(i)d(i) \equiv \boldsymbol{a}\cdot\boldsymbol{d}, \tag{B5}$$

where we have defined $d(i) \equiv \sum_{y<z}\chi^i_{yz}d(y,z)$. In words, $d(i)$ is now the expansion coefficient that indicates how much cycle i contributes to the generalized current j_d.

In analogy with the main text, $I(j_d) \leq I_{\rm quad}(\boldsymbol{p}^*, \boldsymbol{a}^*)$ for any choice of $\boldsymbol{p}^*$ and $\boldsymbol{a}^*$ which satisfy the constraint $\boldsymbol{a}\cdot\boldsymbol{d} = j_d$. We again choose $\boldsymbol{p}^* = \boldsymbol{\pi}$, but now we compute the exact minimizer of the quadratic form $I_{\rm quad}$:

$$\boldsymbol{a}^* = \boldsymbol{a}^\pi + \left(\frac{j_d - j_d^\pi}{\boldsymbol{d}^T G^{-1}\boldsymbol{d}}\right) G^{-1}\boldsymbol{d}. \tag{B6}$$

Hence,

$$I(j_d) \leq \inf_{\boldsymbol{j}|\boldsymbol{j}\cdot\boldsymbol{d}=j_d} I_{\rm quad}(\boldsymbol{\pi}, \boldsymbol{j}) = \frac{(j_d - j_d^\pi)^2}{2\boldsymbol{d}^T G^{-1}\boldsymbol{d}}. \tag{B7}$$

For the coarse-graining problem of Sec. VII, this denominator is simple if we use the cycle basis consisting of the square lattice's plaquettes. Each plaquettes is one of the squares of side length h. Notice that for our coarse-graining procedure, $d(i) = 0$ for all but one of the plaquettes. Only the central plaquette that encircles the origin has a nonzero d. Since we can order the plaquettes arbitrarily, we designate the central plaquette by the label "o" to highlight that it is the plaquette at the origin. Because $d(\mathrm{o}) = 4$, $\boldsymbol{d}^T G^{-1}\boldsymbol{d} = 16 G^{-1}_{\rm oo}$ with $G^{-1}_{\rm oo}$ denoting the diagonal matrix element of G^{-1} for the plaquette at the origin.

Finally, we can see why ϕ is nearly independent of the driving field amplitude A in Fig. 9. In terms of the G matrix,

$$\phi = \left(\frac{2(j_d^\pi)^2}{\mathrm{var}(j_d)}\right)/\Sigma^\pi = \frac{(j_d^\pi)^2}{8 G^{-1}_{\rm oo}\Sigma^\pi}. \tag{B8}$$

For sufficiently small driving amplitude, we anticipate that the mesoscopic currents will respond linearly to the external force: $\boldsymbol{j}^\pi \propto A$. In this linear regime we also have $\boldsymbol{F}^\pi \propto A$, so $\Sigma^\pi \propto A^2$. Furthermore, since G involves ratios of F^p and j, the linear-response value of $G^{-1}_{\rm oo}$ is independent of A. Combining these effects, we see that ϕ does not vary with A in the linear-response regime. Empirically, we observe in Fig. 9 that insensitivity to A in fact extends far beyond the linear-response regime.

[1] S. B. Smith, L. Finzi, and C. Bustamante, Science **258**, 1122 (1992).
[2] V. Blickle and C. Bechinger, Nature Physics **8**, 143 (2012).
[3] I. A. Martínez, E. Roldán, L. Dinis, D. Petrov, J. M. R. Parrondo, and R. A. Rica, Nature Physics **12**, 67 (2016).
[4] U. M. B. Marconi, A. Puglisi, L. Rondoni, and A. Vulpiani, Physics Reports **461**, 111 (2008).
[5] A. Einstein, Annalen der Physik **322**, 549 (1905).
[6] L. Onsager, Physical Review **37**, 405 (1931).
[7] L. Onsager, Physical Review **38**, 2265 (1931).
[8] H. B. Callen and T. A. Welton, Physical Review **83**, 34 (1951).
[9] R. Kubo, Reports on Progress in Physics **29**, 255 (1966).
[10] T. Harada and S.-i. Sasa, Physical Review Letters **95**, 130602 (2005).
[11] T. Speck and U. Seifert, EPL (Europhysics Letters) **74**, 391 (2006).
[12] M. Baiesi, C. Maes, and B. Wynants, Physical Review Letters **103**, 010602 (2009).
[13] J. Prost, J.-F. Joanny, and J. M. R. Parrondo, Physical Review Letters **103**, 090601 (2009).
[14] U. Seifert and T. Speck, EPL (Europhysics Letters) **89**, 10007 (2010).
[15] P. Bohec, F. Gallet, C. Maes, S. Safaverdi, P. Visco, and F. Van Wijland, EPL (Europhysics Letters) **102**, 50005 (2013).
[16] É. Fodor, M. Guo, N. Gov, P. Visco, D. Weitz, and F. van Wijland, EPL (Europhysics Letters) **110**, 48005 (2015).
[17] É. Fodor, W. W. Ahmed, M. Almonacid, M. Bussonnier, N. S. Gov, M.-H. Verlhac, T. Betz, P. Visco, and F. van Wijland, (2015), arXiv:1511.00921 [q-bio].
[18] O. Krichevsky and G. Bonnet, Reports on Progress in Physics **65**, 251 (2002).
[19] G. Kesidis and J. Walrand, IEEE Transactions on Information Theory **39**, 1056 (1993).
[20] C. Maes and K. Netočnỳ, EPL (Europhysics Letters) **82**, 30003 (2008).
[21] L. Bertini, A. Faggionato, and D. Gabrielli, Annales de l'Institut Henri Poincaré. Section B, Probabilités et Statistiques **51**, 867 (2015).
[22] L. Bertini, A. Faggionato, and D. Gabrielli, Stochastic Processes and their Applications **125**, 2786 (2015).
[23] A. C. Barato and U. Seifert, Physical Review Letters **114**, 158101 (2015).
[24] T. R. Gingrich, J. M. Horowitz, N. Perunov, and J. L. England, Physical Review Letters **116**, 120601 (2016).
[25] M. Polettini, A. Lazarescu, and M. Esposito, (2016), arXiv:1605.09692 [cond-mat.stat-mech].
[26] R. Kubo, M. Toda, and N. Hashitsume, *Statistical Physics II: Nonequilibrium Statistical Mechanics*, Vol. 31 (Springer Science & Business Media, 2012).
[27] H. Touchette, Physics Reports **478**, 1 (2009).
[28] N. Van Kampen, *Stochastic Processes in Physics and Chemistry*, Vol. 1 (Elsevier, 1992).
[29] K. H. Hoffmann and P. Salamon, Physica A: Statistical Mechanics and its Applications **390**, 3086 (2011).
[30] M. Esposito, Physical Review E **85**, 041125 (2012).
[31] J. D. Chodera, N. Singhal, V. S. Pande, K. A. Dill, and W. C. Swope, The Journal of Chemical Physics **126**, 155101 (2007).
[32] G. R. Bowman, X. Huang, and V. S. Pande, Methods **49**, 197 (2009).
[33] M. Esposito and C. Van den Broeck, Physical Review E **82**, 011143 (2010).
[34] $F^p(y,z)$ is the difference between the entropy gain of the bath $\Delta S = \ln r(y,z)/r(z,y)$ and the gain in Shannon entropy of the system $\ln p(z)/p(y)$.
[35] D. Chandler, *Introduction to Modern Statistical Mechanics* (Oxford University Press, New York, Oxford, 1987).

[36] Recall that the Poisson point process has $g(t) = 1$.
[37] The initial and final mesostates do not conserve probability, but in the long time limit this effect is insignificant.
[38] Using the monotonicity of arcsinh and the concavity of sinh, Eq. (29) implies that $\partial\Delta/\partial\bar{\jmath} > 0$ for $\bar{\jmath} > 1$ and $\partial\Delta/\partial\bar{\jmath} < 0$ for $0 \leq \bar{\jmath} \leq 1$.
[39] The restriction to conservative currents is build into I because $I(\boldsymbol{p}, \boldsymbol{j}) = \infty$ for non-conservative $\boldsymbol{j}$.
[40] A. C. Barato and R. Chetrite, Journal of Statistical Physics **160**, 1154 (2015).
[41] C. Gardiner, *Stochastic Methods* (Springer Berlin, 2009).
[42] F. Noé, H. Wu, J.-H. Prinz, and N. Plattner, The Journal of Chemical Physics **139**, 184114 (2013).
[43] J. L. Lebowitz and H. Spohn, Journal of Statistical Physics **95**, 333 (1999).
[44] V. Lecomte, C. Appert-Rolland, and F. van Wijland, Journal of Statistical Physics **127**, 51 (2007).
[45] D. E. Smith, S. J. Tans, S. B. Smith, S. Grimes, D. L. Anderson, and C. Bustamante, Nature **413**, 748 (2001).
[46] K. Hayashi, H. Ueno, R. Iino, and H. Noji, Physical Review Letters **104**, 218103 (2010).
[47] C. Maes and K. Netočnỳ, Journal of Mathematical Physics **48**, 053306 (2007).
[48] C. Maes, K. Netocny, and B. Wynants, Markov Processes and Related Fields **14**, 445 (2008).
[49] C. Maes, (2016), arXiv:1603.05147 [cond-mat].
[50] P. Pietzonka, A. C. Barato, and U. Seifert, Journal of Physics A: Mathematical and Theoretical **49**, 34LT01 (2016).
[51] J. Schnakenberg, Reviews of Modern Physics **48**, 571 (1976).